A Diaphragm-Gate Transistor for MEMS Microphones

Mosheh T. Moskowitz
Electrical and Computer Engineering
Johns Hopkins University
3400 North Charles Street
Baltimore, MD 21218
mosheht@eng.umd.edu

Angela M. Hodge
Electronic Science and Tech. Div.
Naval Research Laboratory
4555 Overlook Ave. SW,
Washington, DC 20375
amhodge@eng.umd.edu

Robert W. Newcomb
Dept. of Electrical Engineering
University of Maryland
Microsystems Lab
College Park, MD 20742
newcomb@eng.umd.edu

Abstract -- **We present a process that can be manipulated to build pressure transducers very simply, using standard post fabrication procedure. This process is cost efficient, requiring but one extra step subsequent to standard MOSIS fabrication. Strategically placing hollowed insertions, and filling with hydroflouric acid, allows for the etching of an underlying gate oxide. The resulting cavity turns the layer above it into a diaphragm that produces an output voltage in commensurate with air pressure impingent on the surface. We present an analog circuit used to handle the output signal, and discuss future possibilities for using this device as a microphone.**

I. INTRODUCTION

The first noted mechanical resonator was designed and fabricated at Westinghouse [8], with intentions as a high-Q mechanical resonator. The device consisted of a polarized cantilevered metal beam, vibrating as a result of an input signal controlling an electric field underneath it. Its output was taken from a transistor, whose drain current was controlled by the capacitance formed from the space in between the beam and itself. Modification of the device in [6] and [7] has the beam controlled by air pressure from above, rather than an electric field from underneath. There have been a number of other reports on capacitative microphones, however, they usually incur multiple processing steps, which we consider a shortcoming bypassed with our process [11].

The structure presented here was initially designed to accommodate a secondary function as a fluid-pressure sensor. The details of this application are similar to ours and are discussed in more detail in [3], having proven to strongly differentiate between air, water and Tris/EDTA buffer.

II. DEVICE STRUCTURE AND FABRICATION

The device layout is shown in Fig. 1(a). The initial layout steps are the same as a P-MOS transistor, except for the addition of an extra layer of metal (metal 2) on top. Area on the gate surface is reserved for the concentric rectangles shown in Fig. 1(a), which has center rectangle as open substrate, and outer rectangle as just the p-diffusion over the n-well. These 'holes' in the circuit allow for the deposition of hydrofluoric acid (HF) in order to etch the bottom most oxide layer as shown, resulting in the chip displayed in Fig. 1(b). According to The AMI-Mosis foundry, the gate oxide thickness is approximately 1/1000 μm, or 1 nm given that the permittivity of SiO_2 is 3.45E-11 F/m, (for the remainder of this paper, we use the abbreviation: $X\text{E}Y = X*10^Y$),

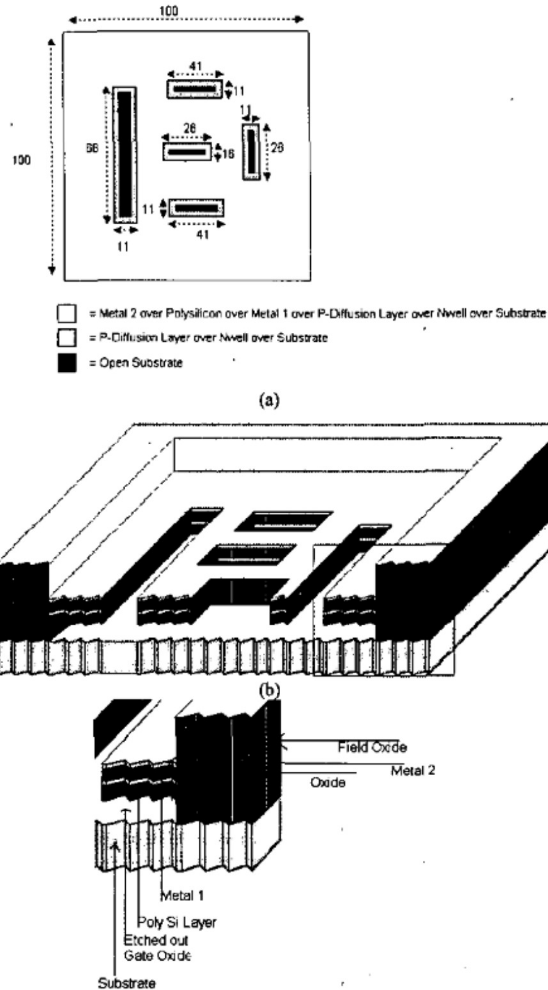

Fig. 1. (a) Layout procedure . (b) Result of (a), lower oxide layer etched out. The layers, from top to bottom are substrate, gate oxide (etched out, about 300E8 m), poly silicon (~1E-6 m thick), metal 1, oxide (~2E-6 m thick), and metal 2. (c) Close up of boxed section in (b).

and that the nominal capacitance per unit area is 44E-18 F/μm^2. The middle oxide layer however is 1 μm, so allowing the etch process to sit for a very brief time will completely etch the lower layer, while hardly touching the middle. Fig. 1(b) shows the gate oxide etched out, and the diaphragm is a

0-7803-7474-6/02/$17.00 ©2002 IEEE

composite of two metal layers, the sandwiched oxide, and the poly silicon layer.

III. THEORY

The conception of using the aforementioned configuration or one of its variances as a microphone/pressure-sensor was validated by finding the center displacement given the average power contained in human speech.

TABLE I
DEFLECTION CALCULATION PARAMETERS

Variable	Value	Units	Description
P	0.1	Pa = N/m²	Pressure
W	1E-4	m	Diaphragm width
L	1E-4	m	Diaphragm length
Th	1.1E-5	m	Thickness
A	1E-8	m	Diaphragm area
I	1.109E-20	m⁴	Moment of inertia
d_{max}	1.677E-14	m	Diaphragm displacement
t_{ox}	3.09E-8	m	Oxide thickness
t_{ox}/d_{max}	1.825E6	m	Thickness/displacement
E	7E10	Pa	Modulus of rigidity (1)
σ_0	1E-3*E	Pa	Elastic limit
α	0.5	Unitless	Max. dist. from center
Δ_{max}	2.273E-7	m	Max. disp.
Δ_{max}/L	2.273E-3	Unitless	Max. disp. per length
Δ_{max}/t_{ox}	7.427	Unitless	Max. disp. per height
ν	0.346	Unitless	Poisson's ratio
M	5.826E-16	Pa/m	Moment at support
R	1.333E6	m	Radius of defl. curv.
G	2.6E10	Pa	Modulus of rigidity (2)
$\tilde{\Delta}$	9.38E-16	m	Displacement approx.

The variables are shown in Table I. *Th*, the thickness, refers to the thickness of the diaphragm, while *d* refers to the height of the support (or the distance in between the bottom of the diaphragm and the base); these are illustrated in Fig. 2. The diaphragm displacement (as a function of impingent pressure) is denoted as Δ. From [4, p. 613, fig. 22.8], we find that the force resulting from a whisper is $P = 0.01$ Pa, and from average volume speech, 0.1 Pa. We take the dimensions of the diaphragm to be $W = L = 1E\text{-}4$. From specifications in [1], we determine the thickness of metal 1 to be 3.5E-6 m, of metal 2, 4E-6 m, and for poly, 3.5E-6. Since the diaphragm is a composite of these layers, its thickness is Th = 1.1e-5 m. We find the force per unit length:

$$f(P) = P \cdot A / L, \tag{3.1}$$

or $f(P)$ = 1e-5. From [9, App. D, p. 701], we find that E=7E10 Pa. From [4, Vol. 3, p. 296], we use the following formula to find the moment of inertia:

$$I = (1/12) \cdot W \cdot Th^3, \tag{3.2}$$

resulting in a value of I = 1.109E-20 m⁴. From [10] and [9, p. 318], we have the maximum displacement (i.e., the displacement in the center of the diaphragm) as:

$$d_{\max}(P) = \frac{5 \cdot f(P) \cdot L^4}{16 \cdot 24 \cdot E \cdot I}, \tag{3.3}$$

which for P = 0.1, gives 1.677E-14.

Comparing with the gate oxide thickness in AMI 1.5μm models from [5, run T24P] shown in Table I, we notice that there are several orders of magnitude ratio between the thickness and displacement, or 1.825E6. The diaphragm displacement required for fracture is [9, p. 316]:

$$\Delta_{\max} = \frac{E}{\sigma_0}\left[1 - \cos\frac{\sigma_0 \cdot L}{2 \cdot E \cdot \alpha \cdot d}\right]. \tag{3.4}$$

Using the values given in Table I, with d = Th, and substituting, we obtain, Δ_{max} = 2.273E-7, Δ_{max}/L = 2.273E-3, and Δ_{max}/t_{ox} = 7.427. We can infer that fracture will not occur since the required distance for it is greater than the oxide thickness; however, deflection due to voice is extremely small. More accurate calculations are given in the appendix that justify using this configuration as a sound sensor. The results given in this section and the appendix are shown in Fig. 3.

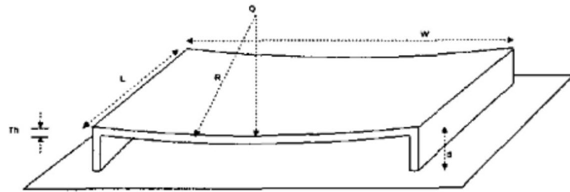

Fig. 2. Beam Geometry.

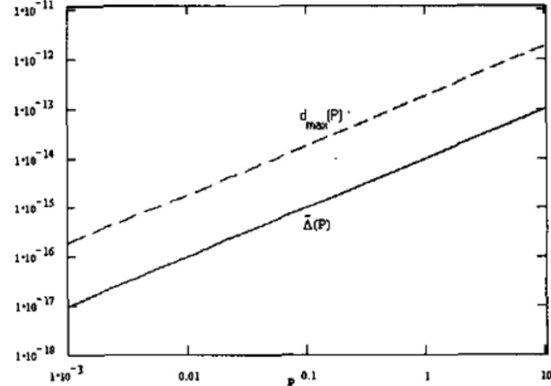

Fig. 3. Diaphragm deflection as a function of pressure. Y-axis in meters, X-axis in pascals.

IV. SIMULATION OF TRANSISTOR PORTION

The standard Spice simulation formulas that are used for the n-MOS transistors and p-MOS microphones are enumerated below and have values summarized in Table II. For the n-MOS:

$$\beta_n = \frac{kp_n}{2}\frac{W_n}{L_n}\frac{1}{\varepsilon_{SiO_2}} \tag{4.1}$$

gives β_n = 9.784E-6.

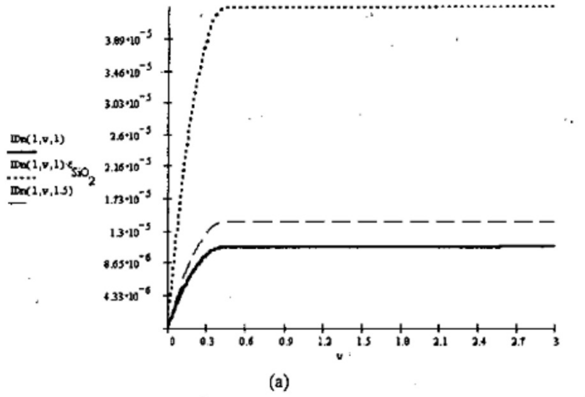

(a)

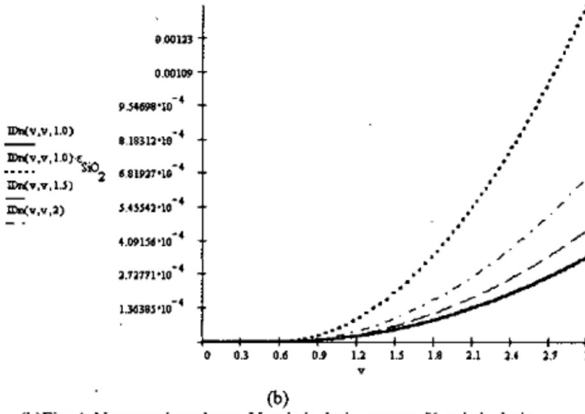

(b)

(b)Fig. 4. N-type microphone. Y-axis is drain current, X-axis is drain voltage: (a) for fixed V_{GS}, and (b), for $V_{GS} = V_D$.

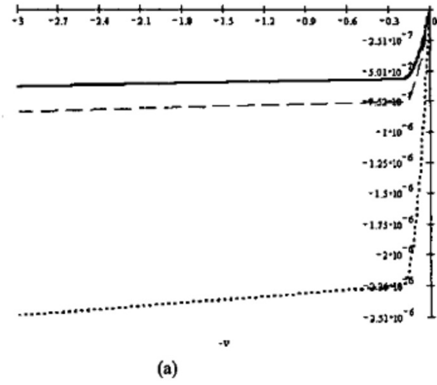

(a)

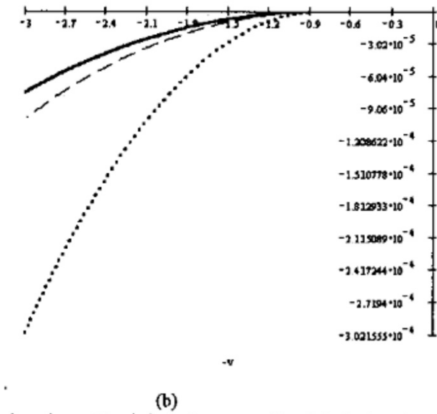

(b)

Fig. 5. P-type microphone. Y-axis is drain current, X-axis is drain voltage: (a) for fixed v_{GS}, and (b), for $v_{GS} = v_D$.

for k_n:

$$k_n(v,d)=\frac{kp_n}{2}\left[\frac{W_n}{L_n}(1+\lambda_n\cdot v)\right]\frac{1}{1-t_{ox}^{-1}\cdot d\cdot 1E-8}\ .\ (4.2)$$

In cutoff mode, the drain current is

$$i_{D_{co}}(v_{GS},v)=0\ . \qquad (4.3)$$

In saturation:

$$i_{D_{sat}}(v_{GS},v,d)=k_n(v,d)\cdot(v_{GS}-v_{to}n)^2\cdot\Phi(v-v_{GS}+v_{to}n) \qquad (4.4),$$

and in ohmic:

$$i_{D_{ohm}}(v_{GS},v,d)=k_n(v,d)\cdot 2\left[(v_{GS}-v_{to}n)\cdot v-v^2\right]\cdot\Phi(v_{GS}-v_{to}n-v) \qquad (4.5).$$

The total drain current is the combination of these:

$$In_D(v_{GS},v,d)=i_{Dco}+\left(i_{Dsat}+i_{Dohm}\right)\cdot\Phi(v_{GS}-v_{to}n)\ . \qquad (4.6)$$

As sample values, In_D (1,3,10) = -3.235E-6 and In_D (2,3,0.1) = 8.296E-5. The simulation runs values of v from 0 to V_{DD} for N-type and $-V_{DD} = V_{SS}$ to 0 for P-type, which are shown in Figs. 4 and 5, respectively. The formulas for the p-type transistors are:

$$\beta_p=\frac{kp_p}{2}\frac{W_p}{L_p}\frac{1}{\varepsilon_{SiO_2}} \qquad (4.7)$$

giving β_p = 3.279E-6, and for k_p:

$$k_p(v,d)=\frac{kp_p}{2}\left[\frac{W_p}{L_p}(1+\lambda_p\cdot v)\right]\frac{1}{1-t_{ox}^{-1}\cdot d\cdot 1E-8}\ . \qquad (4.8)$$

In cutoff mode, the drain current is:

$$i_{D_{co}}(v_{GS},v)=0\ , \qquad (4.9)$$

in saturation:

$$i_{D_{sat}}(v_{GS},v,d)=k_p(v,d)\cdot(v_{GS}-v_{to}p)^2\cdot\Phi(-[v-v_{GS}+v_{to}p]) \qquad (4.10),$$

and in ohmic:

$$i_{D_{ohm}}(v_{GS},v,d)=k_p(v,d)\cdot 2\left[(v_{GS}-v_{to}p)\cdot v-v^2\right]\cdot\Phi(-[v_{GS}-v_{to}n-v]) \qquad (4.11).$$

The total drain current is denoted as:

$$Ip_D(v_{GS},v,d)=i_{Dco}+\left(i_{Dsat}+i_{Dohm}\right)\cdot\Phi(-[v_{GS}-v_{to}p]) \qquad (4.12).$$

The associated curves for these are shown in Fig. 5.

TABLE II
TRANSISTOR-MICROPHONE SIMULATION PARAMETERS

Simulation Variable	Value
kp_n	7.7684E-5
kp_p	1.8891E-5
$v_{to}n$	0.5666
$v_{to}p$	-0.7996
λ_n	1.843E-3
λ_p	4.012E-2
W_n	1E-7
W_p	1E-7
L_n	1E-7
L_p	1E-7
C	1E-12
V_{dd}	3
V_{ss}	-3
T_{ox}	3.06E-8
ε_{air}	1
ε_{SiO2}	3.97

V. OUTPUT PROCESSING CIRCUIT

A balancing circuit is used to account for the bias in the output voltage from the microphone. The circuit is shown in Fig. 6(a), using power voltages of +/- 3V. Notice the form of *W/L* (width to length ratio) for *Mp_sensor*. Because we wish to show the output voltage as a function of the change in oxide thickness (due to the displacement caused by impinging air pressure from the top of the gate), we can more easily account for this change in PSpice by varying the length parameter, rather than changing the oxide thickness from within the parts library. The current will always have the parameter coefficients:

$$\frac{k_p}{2} \cdot \frac{W}{L} = \mu \cdot C_{ox} \cdot \frac{W}{L} = \mu \cdot \varepsilon \cdot \frac{A}{d} \cdot \frac{W}{L} \tag{5.1}$$

where

$$C_{ox} = \varepsilon \frac{A}{d}. \tag{5.2}$$

A change in d is equivalent to a change in L, since they are both in the denominator. Correspondingly, in the simulations dp (in Fig. 6a) is varied from 0 to 1 to account for the change in the gate oxide thickness. The output voltage, *V_out* is shown in Fig. 6b.

VI. DISCUSSION

In experimentation, the chip has been found to be responsive to talking and specifically blowing, yielding a 10-30 mV change in output voltage. These results show promise for future study and variation of this device. Motivation for the conception of this system was two-fold. Originally, this arrangement had been intended as a fluid sensor, and the possibility of using it as a process-inexpensive sound sensor was later verified with cursory testing. Secondly, we are exploring the notion of supplementing current models of the electronic cochlea with more adequate hardware. Several reports have are noted to have similar ideology, such as a contiguous configuration of increasing-frequency resonant beams [11] and an air capacitative transistor as a front-end to an electronic cochlea that produces otoacoustic emissions [6], and a full mechanical cochlea [7]. We are motivated by the biological analogy to the fact that several sound sound-processing calculations thought to have been intelligent, actually occur due almost purely to the mechanics of the basilar membrane hair cells. We envision that by mechanically emulating the function of inner ear stereocilia and basilar membrane, the gap between human and machine hearing will narrow, and perhaps even more undiscovered intelligent functions can be synthesized from a mechanical listening device.

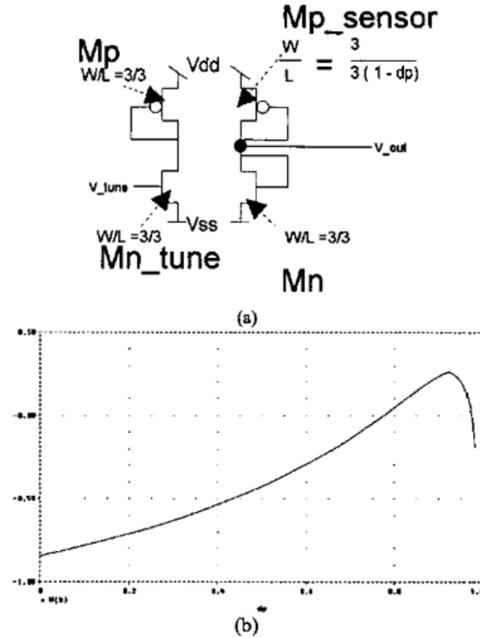

Fig. 6. (a) Bridge balancer for sensor biasing. (b) X-axis is change in dielectric thickness (or length in the simulation), and Y-axis is *V_out* from part (a).

The creation of a device that can closely simulate inner-ear behavior, would putatively be able to simulate muscular behavior and would have further applications to artificial limbs, robotics and the like, once a convenient mechanism is made available to have the processed machinery capable of standing alone from its chip. The previous assumption is based on the fact that both the inner ear and muscle fiber contain active mysosin and actin filaments, powered by ATP hydrolysis. In this case, the myosin moves to the positively charged side on the actin [2]. An equivalent electronic analogy, barring the disposition of nanotechnology (for expense purposes) would consist of an electronic motor made up of parallel plates loosely connected at the ends, so appropriately applied magnetic forces cause them to attract and repel each other, forming inertia, and eventually movement. This requires that the plates have only one degree of freedom, and that they maintain a constant distance between each other.

Future studies with this sort of device will optimize its shape and function to accommodate speech and other slight or higher frequency vibrations.

VII. APPENDIX

To obtain a more accurate calculation for the diaphragm vertical displacement, we start with [9 eq. 4.4.6, p. 126]:

$$\varepsilon_z = \varepsilon_y = -v \cdot \varepsilon_x . \quad \text{(A.1)}$$

Then from [9 p. 701], we find the modulus of rigidity for aluminum is 26G, where G can be calculated using [9, eq. 4.4.14, p. 129]:

$$v = \frac{E}{2 \cdot G} - 1 \quad \text{(A.2)}$$

with v = 0.346. Using 7E10 Pa for the value of E, G is found to be 2.6E10. From [9, p. 248, eq. 8.6.9d]:

$$\varepsilon_y = -v \frac{M_z \cdot y}{E \cdot I_{zz}} \quad \text{(A.3)}$$

or

$$M_z = \varepsilon_y \frac{E \cdot I_{zz}}{-v \cdot y} \quad \text{(A.4)}$$

and from [1, p. 258, eq. 8.6.9b], the stress is

$$\sigma_x(y) = \frac{M_z \cdot y}{I_{zz}} . \quad \text{(A.5)}$$

R, the radius of curvature (the inverse of the curvature), is [9, p. 258, eq. 8.6.9a]:

$$R = \frac{E \cdot I_{zz}}{M_z}, \quad \text{(A.6)}$$

so

$$R = \frac{E \cdot I_{zz}}{\varepsilon_y \frac{E \cdot I_{zz}}{v \cdot Th/2}} = \frac{v \cdot Th/2}{\varepsilon_y} = \frac{v \cdot Th/2}{\sigma_x / E}, \quad \text{(A.7)}$$

and

$$R(P) = \frac{v \cdot E \cdot Th/2}{P} . \quad \text{(A.8)}$$

We find the moment:

$$M(P) = \frac{P \cdot I}{v \cdot Th/2}, \quad \text{(A.9)}$$

again using P = 0.1, giving $M(P{=}0.1)$ = 5.826E-16. Using [9 p. 251, eq. 8.6.13], we have:

$$\Delta(P) = R(P)\left[1 - \cos\left(\frac{L}{2 \cdot R(P)}\right)\right], \quad \text{(A.10)}$$

and using the expanded form of cosine:

$$\cos x = 1 - \frac{x^2}{2} + \ldots, \quad \text{(A.11)}$$

gives a further approximation of the displacement:

$$\tilde{\Delta} = \frac{R}{2} \cdot \left(\frac{L}{2 \cdot R}\right)^2 = \frac{L^2}{8 \cdot R(P)} \quad \text{(A.12)}$$

or 9.38E-16.

Some factors for improvement we consider, is that the beam can be fabricated to be a maximum of 1400 um (in contrast to the 100 um we originally fabricated), and affects the L^2 term. Thinning the beam to poly silicon, gives a smaller Th, 3.5E-6 m, and lowers the modulus of elasticity to 20G, or 2E10, which substituting into (A.12) gives $\tilde{\Delta} = 4.044E-12$. To get a more reasonable value, we use the linear formulation:

$$I = \frac{1}{12} W \cdot Th^2 = 3.573E-22 . \quad \text{(A.13)}$$

Proceeding similarly to (3.3), we obtain $\Delta_{max} = 7E-8$. We hypothesize that arranging many of these devices in parallel may improve future performance.

VIII. REFERENCES

[1] AMI Semiconductor, Foundary: AMIS AB-1.5/3.5 Process Family Technologies data, http://www.amis.com/ foundary/ process.cfm

[2] F. Julicher, "Force and motion generation of molecular motors: a generic description," in *Lecture Notes in Physics: Transport and Structure: Their Competitive Roles in Biophysics and Chemistry*, ed. S. C. Muller, J. Parisi and W. Zimmerman, Springer, Berlin 1999.

[3] A. M. Hodge, R. W. Newcomb, "Evaluation of the VLSI adaptation of a the Chemfet, a biosensor for fluid analysis," in *Proc. Int. Symp. Circ. and Syst.*, Phoenix, AZ USA, 2: 580-583, May 2002.

[4] L. S. Lerner, *Physics for Scientists and Engineers*, Jones and Bartlett Publishers, Boston, 1996.

[5] Mosis data web page: http://www.mosis.org/ Technical/Testdata/ami-abn-prm.html.

[6] Moskowitz MT, Sellami L, Newcomb RW, Rodellar V, "Current mode realization of ear-type multisensors," in *Proc. Int. Symp. Circ. and Syst.*, Sydney, Australia, 2:285-288, May 2001.

[7] Moskowitz MT, Sellami L, Rodellar V, Newcomb RW, "A novel resonant microphone transduction mechanism for use in the scattering cochlea model," in *Proc. Conf. on Info. Sci. and Syst., Johns Hopkins University*, Baltimore, MD USA, 2:329-333, March 2001.

[8] H. C. Nathanson, W. E. Newell, R. A. Wickstrom, J. R. Davis Jr., "The resonant gate transistor," *IEEE Trans. Elect. Dev.*, ED-14(3): 117-133, March 1967.

[9] R. Parnes, *Solid Mechanics in Engineering*, John Wiley and Sons, 2001.

[10] A. Sommerfeld, *Lectures on Theoretical Physics*, Academic Press, New York, 1950.

[11] K. Tanaka, M. Abe, S. Ando, "A novel mechanical cochlea 'fishbone' with dual sensor/actuator characteristics," *IEEE/ASME Trans. on Mechatron.*. 3(2): 98-105, June 1998.